Polarization-dependent aluminum metasurface operating at 450 nm

Højlund-Nielsen, Emil; Zhu, Xiaolong; Carstensen, Marcus S; Sørensen, Michael K; Vannahme, Christoph; Mortensen, N. Asger; Kristensen, Anders

Published in:
Optics Express

Link to article, DOI:
10.1364/oe.23.028829

Publication date:
2015

Document Version
Publisher's PDF, also known as Version of record

Polarization-dependent aluminum metasurface operating at 450 nm

Emil Højlund-Nielsen,[1] Xiaolong Zhu,[1] Marcus S. Carstensen,[1] Michael K. Sørensen,[1] Christoph Vannahme,[1] N. Asger Mortensen, and [2] Anders Kristensen[1,*]

[1]*Technical University of Denmark, DTU Nanotech, Ørsteds Plads, DK-2800 Kgs. Lyngby, Denmark*

[2]*Technical University of Denmark, DTU Fotonik, Ørsteds Plads, DK-2800 Kgs. Lyngby, Denmark*

anders.kristensen@nanotech.dtu.dk

Abstract: We report on a polarization-dependent plasmonic aluminum-based high-density metasurface operating at blue wavelengths. The fabricated sub-wavelength structures, tailored in size and geometry, possess strong, localized, plasmonic resonances able to control linear polarization. Best performance is achieved by rotating an elongated rectangular structure of length 180 nm and width 110 nm inside a square lattice of period 250 nm. In the case of 45 degrees rotation of the structure with respect to the lattice, the normal-incidence reflectance drops around the resonance wavelength of 457 nm from about 60 percent to below 2 percent.

OCIS codes: (130.5440) Polarization-selective devices; (050.6624) Subwavelength structures; (220.0220) Optical design and fabrication; (240.6680) Surface plasmons.

References and links

1. X. M. Goh, Y. Zheng, S. J. Tan, L. Zhang, K. Kumar, C.-W. Qiu, and J. K. W. Yang, "Three-dimensional plasmonic stereoscopic prints in full colour," Nat. Commun. **5**, 5361 (2014).
2. E. Petryayeva and U. J. Krull, "Localized surface plasmon resonance: nanostructures, bioassays and biosensing - a review," Anal. Chim. Acta **706**, 8–24 (2011).
3. R. Gans, "Über die Form ultramikroskopischer Goldteilchen," Ann. Phys. **342**, 881–900 (1912).
4. G. Papavassiliou, "Optical properties of small inorganic and organic metal particles," Prog. Solid State Chem. **12**, 185–271 (1979).
5. S. Link and M. A. El-Sayed, "Shape and size dependence of radiative, non-radiative and photothermal properties of gold nanocrystals," Int. Rev. Phys. Chem. **19**, 409–453 (2000).
6. F.-J. Haug, T. Soderstrom, O. Cubero, V. Terrazzoni-Daudrix, and C. Ballif, "Plasmonic absorption in textured silver back reflectors of thin film solar cells," J. Appl. Phys. **104**, 064509 (2008).
7. F. Le, D. W. Brandl, Y. A. Urzhumov, H. Wang, J. Kundu, N. J. Halas, J. Aizpurua, and P. Nordlander, "Metallic nanoparticle arrays: a common substrate for both surface-enhanced Raman scattering and surface-enhanced infrared absorption," ACS Nano **2**, 707–718 (2008).
8. R. Adato, A. A. Yanik, J. J. Amsden, D. L. Kaplan, F. G. Omenetto, M. K. Hong, S. Erramilli, and H. Altug, "Ultra-sensitive vibrational spectroscopy of protein monolayers with plasmonic nanoantenna arrays," Proc. Natl. Acad. Sci. U. S. A. **106**, 19227–19232 (2009).
9. X. Zhu, S. Xiao, L. Shi, X. Liu, J. Zi, O. Hansen, and N. A. Mortensen, "A stretch-tunable plasmonic structure with a polarization-dependent response," Opt. Express **20**, 5237 (2012).
10. W. Chen, M. Tymchenko, P. Gopalan, X. Ye, Y. Wu, M. Zhang, C. B. Murray, A. Alu, and C. R. Kagan, "Large-area nanoimprinted colloidal Au nanocrystal-based nanoantennas for ultrathin polarizing plasmonic metasurfaces," Nano Lett. **15**, 5254–5260 (2015).
11. M. E. Stewart, C. R. Anderton, L. B. Thompson, J. Maria, S. K. Gray, J. A. Rogers, and R. G. Nuzzo, "Nanostructured plasmonic sensors," Chem. Rev. **108**, 494–521 (2008).

#249212 Received 15 Sep 2015; revised 15 Oct 2015; accepted 21 Oct 2015; published 27 Oct 2015

12. H. Lu, X. Liu, D. Mao, and G. Wang, "Plasmonic nanosensor based on Fano resonance in waveguide-coupled resonators," Opt. Lett. **37**, 3780 (2012).
13. D. Gérard and S. K. Gray, "Aluminium plasmonics," J. Phys. D. Appl. Phys. **184001**, 184001 (2015).
14. A. L. Ramaswamy and P. Kaste, "A nanovision of the physiochemical phenomena occurring in nanoparticles of aluminum," J. Energ. Mater. **23**, 1–25 (2005).
15. L. Jeurgens, W. Sloof, F. Tichelaar, and E. Mittemeijer, "Thermodynamic stability of amorphous oxide films on metals: application to aluminum oxide films on aluminum substrates," Phys. Rev. B **62**, 4707–4719 (2000).
16. G. H. Chan, J. Zhao, G. C. Schatz, and R. P. Van Duyne, "Localized surface plasmon resonance spectroscopy of triangular aluminum nanoparticles," J. Phys. Chem. C **112**, 13958–13963 (2008).
17. P. West, S. Ishii, G. Naik, N. Emani, V. Shalaev, and A. Boltasseva, "Searching for better plasmonic materials," Laser Photonics Rev. **4**, 795–808 (2010).
18. J. Zhang, J.-Y. Ou, N. Papasimakis, Y. Chen, K. F. MacDonald, and N. I. Zheludev, "Continuous metal plasmonic frequency selective surfaces," Opt. Express **19**, 23279–23285 (2011).
19. C. Langhammer, M. Schwind, B. Kasemo, and I. Zorić, "Localized surface plasmon resonances in aluminum nanodisks," Nano Lett. **8**, 1461–1471 (2008).
20. M. W. Knight, N. S. King, L. Liu, H. O. Everitt, P. Nordlander, and N. J. Halas, "Aluminum for plasmonics," ACS Nano **8**, 834–840 (2014).
21. I. Zorić, M. Zäch, B. Kasemo, and C. Langhammer, "Gold, platinum, and aluminum nanodisk plasmons: material independence, subradiance, and damping mechanisms," ACS Nano **5**, 2535–2546 (2011).
22. S. J. Tan, L. Zhang, D. Zhu, X. M. Goh, Y. M. Wang, K. Kumar, C.-W. Qiu, and J. K. W. Yang, "Plasmonic color palettes for photorealistic printing with aluminum nanostructures," Nano Lett. **14**, 4023–4029 (2014).
23. H. Lochbihler, "Reflective colored image based on metal-dielectric-metal-coated gratings," Opt. Lett. **38**, 1398–1400 (2013).
24. J. Olson, A. Manjavacas, L. Liu, W.-S. Chang, B. Foerster, N. S. King, M. W. Knight, P. Nordlander, N. J. Halas, and S. Link, "Vivid, full-color aluminum plasmonic pixels," Proc. Natl. Acad. Sci. U.S.A. **111**, 14348–14353 (2014).
25. E. Prodan, C. Radloff, N. J. Halas, and P. Nordlander, "A hybridization model for the plasmon response of complex nanostructures," Science **302**, 419–422 (2003).
26. J. S. Clausen, E. Højlund-Nielsen, A. B. Christiansen, S. Yazdi, M. Grajower, H. Taha, U. Levy, A. Kristensen, and N. A. Mortensen, "Plasmonic metasurfaces for coloration of plastic consumer products," Nano Lett. **14**, 4499–4504 (2014).
27. C. Vannahme, M. Dufva, and A. Kristensen, "High frame rate multi-resonance imaging refractometry with distributed feedback dye laser sensor," Light Sci. Appl. **4**, e269 (2015).
28. P. G. Hermannsson, K. T. Sørensen, C. Vannahme, C. L. Smith, J. J. Klein, M.-M. Russew, G. Grützner, and A. Kristensen, "All-polymer photonic crystal slab sensor," Opt. Express **23**, 16529 (2015).
29. M. A. Green and M. J. Keevers, "Optical properties of intrinsic silicon at 300 K," Prog. Photovoltaics Res. Appl. **3**, 189–192 (1995).
30. E. Højlund-Nielsen, J. Weirich, J. Nørregaard, J. Garnaes, N. A. Mortensen, and A. Kristensen, "Angle-independent structural colors of silicon," J. Nanophotonics **8**, 083988 (2014).
31. S. Raza, S. I. Bozhevolnyi, M. Wubs, and N. A. Mortensen , "Nonlocal optical response in metallic nanostructures," J. Phys. Condens. Matter **27**, 183204 (2015).
32. E. Palik, *Handbook of Optical Constants of Solids* (Academic Press, 1986).

1. Introduction

The polarization of light is a fundamental attribute of electromagnetic waves, providing information about its spacial travel direction and clues to its past. Polarization properties have interesting applications within display technologies, high-density optical storage, anti-counterfeiting and bio-sensing [1, 2]. Here we present a polarization dependent plasmonic aluminum-based high-density metasurface operating at blue wavelengths. The sensory element performs in reflection mode and provides the possibility to detect polarization information by visual means.

The polarization dependent metasurface described here is based on sub-wavelength plasmonic rectangular structures. Similar freely suspended elongated ellipsoidal nanoparticles were first described as polarization dependent in 1912 by Gans [3], that predicted the splitting of surface plasmons into two distinct oscillation modes, namely the high-energy tranverse and the low-energy longitudinal oscillation of conduction band electrons [4, 5]. Unfortunately, freely suspended particles lack precise orientation control, which limits filter resolution.

In contrast, microfabricated plasmonic metasurfaces allow individual control of the shape,

#249212 Received 15 Sep 2015; revised 15 Oct 2015; accepted 21 Oct 2015; published 27 Oct 2015

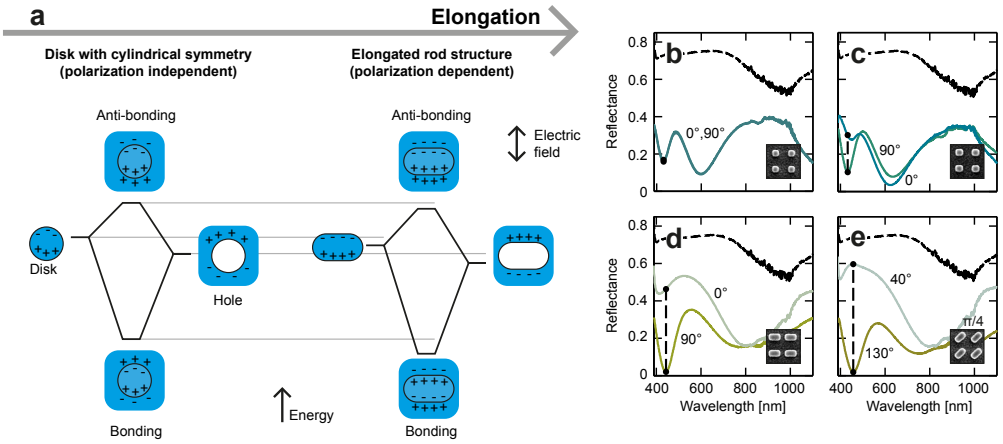

Fig. 1. Hybrid transverse mode concept by elongation of base plasmonic structure. a) Energy hybridization diagrams of circular and elongated structures at transverse polarization. b-e Representative reflectance spectra for different polarizations of various structures with CIE/sRGB calculated color coding. Top dashed lines show spectrum for non-structured surface.

position and orientation of the active entities. In particular, two-dimensional metasurfaces of well-controlled spatial arrangements have attracted considerable attention over the last two decades for their simple design and fabrication, and for their ability to enhance electromagnetic fields. Metasurfaces have been demonstrated to manipulate visible and infrared absorption [6–8] at high polarization conversion efficiencies for sensor applications [9–12].

Aluminum has attractive properties compared to typical plasmonic materials [13], such as silver and gold, due to its natural abundance, low cost, protective oxide layer for high durability [14–16] and plasmonic properties in the visible range [17–21]. Based on aluminum, reflective plasmonic colors utilizing the concept of localized surface plasmon resonances (LSPR) have been presented [22–24] and the hybridization between LSPR modes [25] has been used to design and fabricate polarization independent colors [26]. Polarization dependent aluminum metasurfaces have also been demonstrated for full-color stereoscopic printing by Goh *et al.* [1]. However the metasurface was based on electron beam lithography in HSQ directly on a silicon substrate, impeding fabrication scalability. Furthermore, the ellipse dimensions were varied from 100 nm to 190 nm within a lattice of period 400-500 nm, which indicates poor color contrast and angular dependence.

We present a similar ultra-thin high-density platform, however with a sub-wavelength period of 250 nm for better angular insensitivity and fabricated by a scalable nanoreplication process in hybrid polymer. Compared to Goh *et al.* [1], the presented platform is about four times smaller per unit-cell, mass-producible, and constitutes an important step towards application of polarization-dependent metasurfaces.

To enhance the performance of the metasurface, we rotate the structure with respect to the square lattice in order to elongate the plasmonic structure and increase the resonance strength. The concept of elongation and rotation of the base structure to utilize the hybrid transverse mode is illustrated in Fig. 1. In Fig. 1(a), energy hybridization diagrams for the transverse mode and the structure itself are sketched. In Figs. 1(b)-(e), typical reflectance spectra for different polarizations of various structures (insets) are plotted using CIE/sRGB calculated color coding (see Section 3 for experimental details). The resonance enhancement by rotation of the polarization-dependent resonance behavior around 450 nm is clearly seen.

#249212 Received 15 Sep 2015; revised 15 Oct 2015; accepted 21 Oct 2015; published 27 Oct 2015

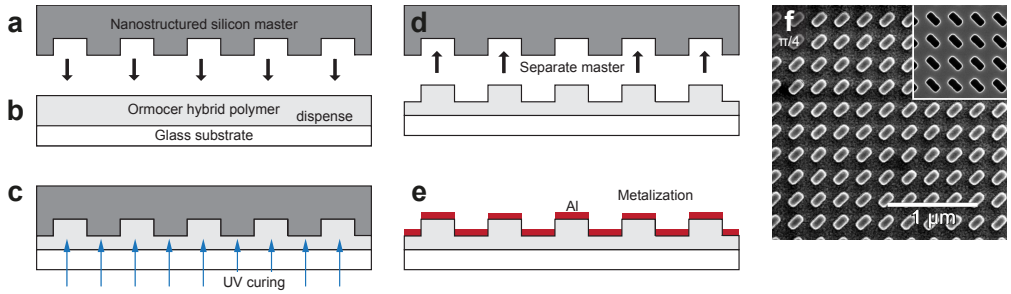

Fig. 2. Fabrication process for 250 nm periodic structures from pattern definition to metalized polymer replica. a-e) Sketch of fabrication process, see text. f) SEM image of metalized polymer replica for 45° rotation inside unit-cell. Corresponding SEM image of Si master can be seen as inset.

2. Fabrication

The plasmonic color filter was fabricated by UV nanoreplication, as sketched in Figs. 2(a)-(e). A silicon master containing areas with two-dimensional periodic structures was fabricated by electron beam lithography and dry etching, see Fig. 2(a). The master was anti-stiction coated with a few monolayers of perfluorodecyltrichlorosilane (FDTS) using molecular vapor deposition.

The sample replica was prepared by dispensing an UV curable hybrid polymer (OrmoComp, Micro Resist Technology GmbH, Germany) onto a borosilicate glass wafer acting as carrier substrate, see Fig. 2(b). The master was brought into contact with the soft hybrid polymer between the opaque silicon master and the transparent glass substrate. The polymer was cured by ultra-violet (UV) light through the glass substrate for 18 min, as shown in Fig. 2(c). After curing, the master and the hybrid polymer were manually separated, leaving the solidified hybrid material on the glass substrate with a nano-structured surface created as a negative of the master pattern, see Fig. 2(d). Finally, a 18 nm thin film of aluminum was deposited on top of the structure by electron beam evaporation in vacuum at a rate of about 1.0 nm/s. The vertical side walls and the height differences of about 50 nm of the polymer topography lead to the formation of isolated metal islands on top of the polymer pillars, as seen in Fig. 2(d).

Representative SEM images of patterns on the polymer replica and the corresponding master area can be seen in Fig. 2(f). The mirror symmetry between master and replica due to the replication process can be seen. The rectangular structures are rounded at the corners. In general, the fabrication process was optimized for a high yield and SEM inspections of the master and final samples did not reveal defects or pattern deviations.

3. Experiments

Figure 3 presents the experimental results. In Fig. 3(a), the polarization angle and the rotation angle of the structure are defined with respect to the basis lattice vector of the square lattice (x-axis). Normal incidence reflectance spectra were obtained for the metalized polymer samples using a modification of an experimental setup previously used for photonic crystal characterization [27, 28].

The setup is schematically illustrated in Fig. 3(b). Light from a broadband laser-driven light source (Energetiq EQ-99XFC) was fed to the setup via an optical fiber and collimated with a fiber collimator. A linear polarizer on a rotational stage was used to control the polarization of the light. The light was then focused with a lens and reflected into a 10x microscope objective by a beam splitter. The light then emerged collimated from the other side of the ob-

#249212 Received 15 Sep 2015; revised 15 Oct 2015; accepted 21 Oct 2015; published 27 Oct 2015

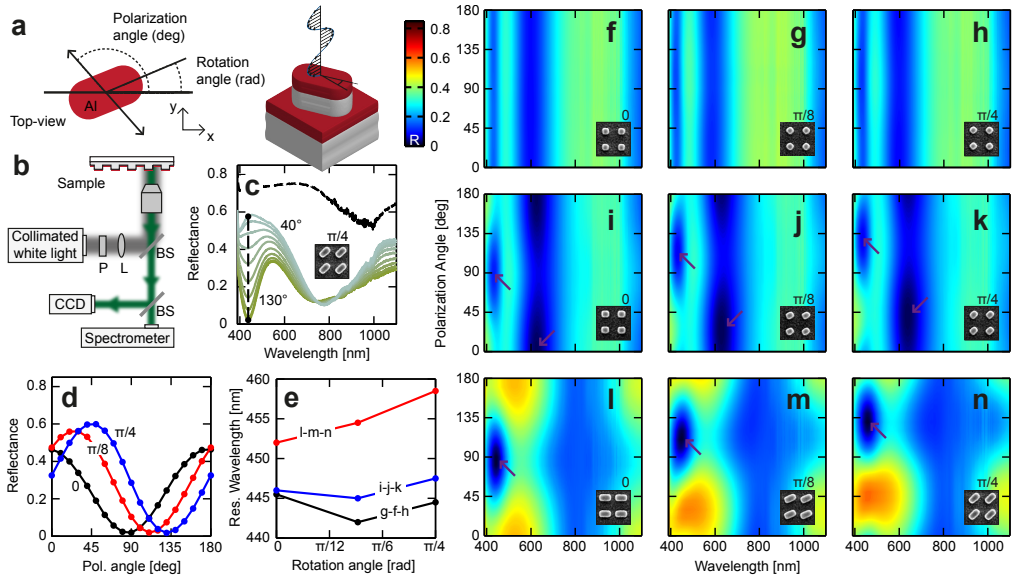

Fig. 3. Measured normal incidence reflectance spectra for metalized polymer samples. a) Definition of coordinate system and angles. b) Schematic illustration of optical setup. c) Reflectance as function of wavelength for different polarizations in the case of structure "n" with CIE/sRGB calculated color coding. Top dashed line shows spectrum for non-structured surface. d) Reflectance as function of polarization angle at resonance wavelength for elongated structures "l", "m", and "n". e) Resonance wavelengths as function of rotation angle. f-n) Reflectance as function of wavelength and polarization angle for all nine investigated topographies. Arrows indicate transverse (450 nm) and longitudinal (630 nm) resonances.

jective and illuminated the device at normal incidence. The reflected light traveled backwards through the objective and beam splitter and was then simultaneously focused by a microscope tube lens onto the slit of an imaging spectrometer (Acton SP-2756 Imaging Spectrograph with PIXIS100B Digital built-in camera and grating 150 g/mm) and a CCD camera via another beam splitter. Thus, positioning was controlled and recorded with the CCD camera while the reflected spectrum was analyzed with the spectrometer. Intensity counts were acquired from the spectrometer and signal counts were calculated by subtracting corresponding dark background spectra. In order to calculate the absolute reflectance, polished silicon was used as reference using well-established tabulated optical properties of silicon [29]. The reflectance was calculated as function of wavelength depending on polarization angle for a given sample area.

In Fig. 3(c), reflectance spectra for different polarization angles are shown for the structures seen in Fig. 2(f), respectively. The spectra are represented by calculated colors using a previously described methodology [30], where the reflectance is converted to a CIE XYZ color using a standard D65 light source and 2° CIE observer, and finally converted to sRGB color space for screen viewing. The resulting reflectance depends strongly on polarization. In Fig. 3(d), the reflectance is plotted as function of polarization angle at resonance wavelength for the series of elongated structures seen as insets in Figs. 3(l)-(n). In Fig. 3(e) the corresponding resonance wavelengths are plotted. Finally, in order to provide an overview, Figs. 3(f)-(n) visualize the reflectance spectra using contour-plots for different polarization angles for all nine investigated topographies with corresponding SEM images as insets.

#249212 Received 15 Sep 2015; revised 15 Oct 2015; accepted 21 Oct 2015; published 27 Oct 2015

4. Numerical simulations

In order to support the experimental findings, simulations were conducted using a frequency-domain solver with periodic boundary conditions in the surface plane (CST Microwave Studio). Despite the nanometric dimensions, the smallest characteristic features are still sufficiently large to allow classical electrodynamics considerations [31]. Normal to the structures, the simulation domain was extending 300 nm away from the metal and at the boundaries Floquet ports were used. The frequency-dependent permittivity used for aluminum were from the handbook of Palik [32]. Substrate and coating were assumed to have a refractive index of 1.5.

Figure 4 presents the simulation results. In Fig. 4(a) the corresponding reflectance spectra of the structures in Fig. 2(n) at 40° and 130° polarization angle are seen, showing good agreement with the experimental results. In Fig. 4(b) the detailed 2D simulated reflectance spectra of the structures in Fig. 2(f) are seen, showing the resonance evolution with similar trends as seen in Fig. 3(n). In order to further illustrate this, an absolute field profile is presented in Fig. 4(c) based on the scaling seen in Fig. 4(d).

Based on the scaling seen in Fig. 4(e), the z-component of the electric field cross-section profiles in the center of the patches can be seen in Figs. 4(f)-4(n). The unit cell supports complex field distributions extending both into the metalair interface and the surroundings. This mode corresponds to a hybrid transverse mode resonating along the short axis of the plasmonic structure with a strong coupling at its resonant frequency. Eventually these plasmonic resonances presented here lead to the enhanced absorption and thereby reduced reflection. As a result, at the frequencies of these modes, the electric field concentrates at the sharp corners (as shown in the corresponding insets in Figs. 4(f)-4(n) and in Fig. 4(c)), which support a strong enhancement of the localized fields.

5. Discussion

From the experimental and numerical simulation results, a number of trends can be observed. First, two resonances can be observed for rounded-square structures, see Fig. 3(f). These resonances correspond to the well-known hybridization between LSPR modes [25] in aluminum nanodisks and nanoholes. The high energy resonance in the blue part of the spectra is seen to be more spectrally narrow than the low energy resonance in the red part of the visual spectrum. It is also clear that rotating the 100 nm rounded-square structure does not disturb the hybridization between the polarization-independent LSPR modes and hence no significant dependence of the reflectance on polarization angle can be observed, see Figs. 3(g)-3(h).

Secondly, elongating the base structures about 25 nm in one direction causes the reflectance to become somewhat polarization dependent, see Fig. 3(b). The high energy resonance is present when the polarized light is perpendicular to the base structure, e.g. at 90° for structure ”i”, see Fig. 3(i). The reflectance minimum follows accordingly for rotation of the rectangular structure with respect to the lattice, such that the minimum reflectance around a wavelength of 450 nm shifts to 135° for structure ”k” with rotation 45°, see. Fig. 3(k). This clearly indicates that the polarization dependence is connected to a transverse plasmonic mode of the metal disks.

Finally, elongating the length to about 190 nm (width ca. 110 nm) causes the reflectance at blue wavelengths to become strongly polarization dependent, see Fig. 3(l). It is also clear that the resonance strength is clearly enhanced, while the reflectance off-resonance is also higher. By elongating the plasmonic base structure, the hybridization modes become polarization dependent, such that the high energy mode has the character of a hybrid transverse mode. This is also seen in the simulations, see Fig 4(l). By rotation of the base structure, the resonance strength is further improved and the resonance wavelength increases slightly. In the case of 45° rotation angle for structure ”n”, the normal-incidence reflectance drops around the blue reso-

#249212 Received 15 Sep 2015; revised 15 Oct 2015; accepted 21 Oct 2015; published 27 Oct 2015

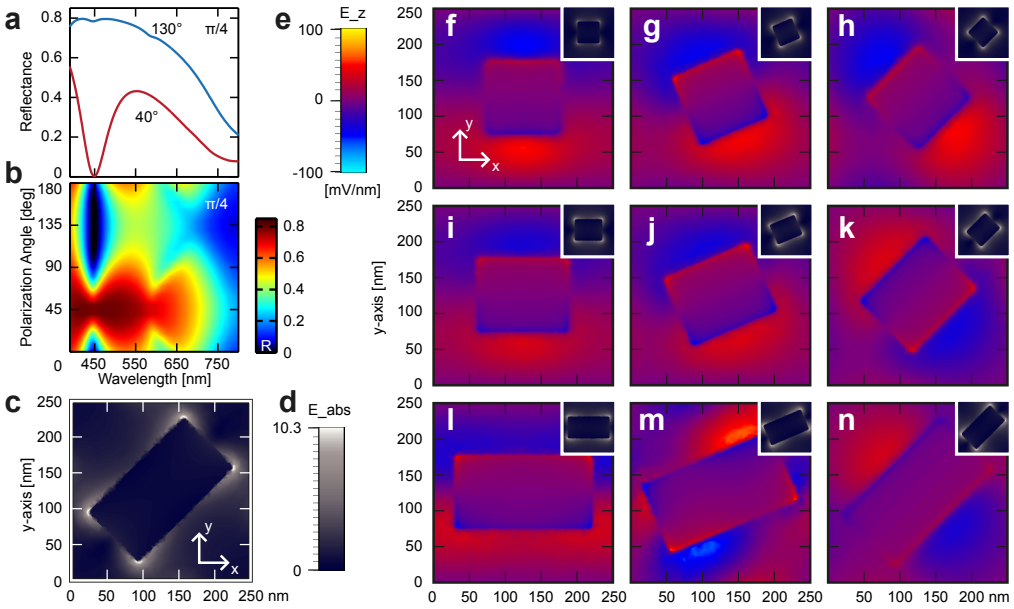

Fig. 4. Simulations. a) Reflectance spectra for structure "n" at 40° and 130° polarization angle. b) Reflectance contour-plot for structure "n". c) Absolute electric field intensity for structure "n". d) Scale for absolute field intensity with maximum of 800 mV/nm. e) Scale for z-component of electric field for input field of 76.6 mV/nm. f-n) Plots of the electric field z-component inside the unit-cell, with inserts of the corresponding absolute field intensity for structures "f"-"n" at the high-energy resonance for optimal polarization angle (90°, 113°, 135°) and phase. The hybrid transverse mode can be seen.

nance wavelength (457 nm) from about 60% to below 1.6%. This "on/off" ratio of 33.4 creates a visible color discrepancy, see Fig 3(b). This agrees well with the simulations, see Fig 4(n).

6. Conclusion

In conclusion, we reported on a polarization dependent plasmonic aluminum-based metasurface operating at blue wavelengths. The fabricated subwavelength structures, displayed strong, localized, plasmonic resonances able to control linear polarization. Best performance was acheived by rotating an elongated rectangular structure of length 180 nm and width 110 nm inside a square lattice of period 250 nm. In the case of 45° rotation of the structure with respect to the lattice, the normal-incidence reflectance decreased around the resonance wavelength of 457 nm from about 60 percent to below 2 percent with a ratio of 33, thereby providing on/off controllability of reflectance for detection of polarized UV-visual light.

Acknowledgments

This work was supported by the European Commission via the FP7 MMP Integrated project Plast4Future (NMP2-SE-2012-314345).

#249212 Received 15 Sep 2015; revised 15 Oct 2015; accepted 21 Oct 2015; published 27 Oct 2015